Scientific Research Publishing

Open Journal of Geology, 2023, 13, 1007-1023
https://www.scirp.org/journal/ojg
ISSN Online: 2161-7589
ISSN Print: 2161-7570

Cu-Bearing Mokama Granite Prospect of the Kibara Belt in the Maniema Province, DRC: A Preliminary Petrography, Geochemistry, and Fluid Inclusion Study

Douxdoux Kumakele Makutu[1,2*], Ivan Bongwe[2], Chris Musomo Mfumu[2], Frederick Makoka Mwanza[2], Jean-Pierre Bulambo[3], Pierre Kambuli Kaseti[3]

[1]Energy Resource Department, College of Engineering, Inha University, Incheon, Republic of Korea
[2]Department of Geosciences, Kinshasa University, Kinshasa, Democratic Republic of the Congo
[3]Department of Geology, University of Lubumbashi, Lubumbashi, Democratic Republic of the Congo
Email: *dx7itaewon@gmail.com, grevanabons@gmail.com, spinellechris@gmail.com, makokamfre@gmail.com, Bulambojeanpierre2@gmail.com, pierrkaseti@gmail.com

How to cite this paper: Makutu, D.K., Bongwe, I., Mfumu, C.M., Mwanza, F.M., Bulambo, J.-P. and Kaseti, P.K. (2023) Cu-Bearing Mokama Granite Prospect of the Kibara Belt in the Maniema Province, DRC: A Preliminary Petrography, Geochemistry, and Fluid Inclusion Study. *Open Journal of Geology*, **13**, 1007-1023.
https://doi.org/10.4236/ojg.2023.1310043

Received: September 7, 2023
Accepted: October 8, 2023
Published: October 11, 2023

Abstract

The Mokama granites are located in the Kibara belt (KIB) and hosts tin oxide group minerals (TOGM: Sn-W), and sulfide group minerals (SGM: Cu-Zn-Fe-As). The essential of Cu mineralization (non-economic deposit) is disseminated inside the rock and consists of minerals (Raman, EPMA and metallographic microscopy) including chalcopyrite and bornite that are replaced by chalcocite and covellite, and the last also replaced later by malachite. The chemistry (XRF, LA-ICP-MS) of these peraluminous S-type leucogranites show SiO_2 (71 wt% - 79 wt%), ASI (1.4 - 3.1 molar), and are enriched in Rb (681 - 1000 ppm), Ta (12–151 ppm), Sn (43 - 142 ppm), Cu (10 - 4300 ppm), Zn (60 - 740 ppm), U (2.2 - 20.7 ppm) while depleted in Zr (20 - 31 ppm), Sr (20 - 69 ppm), Hf (1.3 - 2.0 ppm), Th (2.2 - 18.9 ppm), W (9 - 113 ppm), Pb (5 - 50 ppm), Ge (5 - 10 ppm), Cs (21 - 53 ppm) and Bi (0.6 - 17.4 ppm) and low ratios of (La/Yb) N, (Gd/Yb) N, (La/Sm) N). Fluid inclusion assemblages (FIAs) hosted in quartz in the Mokama granites show ranges of salinities of 4 - 23 wt% (NaCl equivalent) and homogenization temperatures (Th) of 190˚C - 550˚C. A boiling assemblage in the granite suggests a fluid phase separation occurred at about 380 - 610 bars, and this corresponds to apparent paleodepths of approximately 1 - 2 km (lithostatic model) or 3 - 5 km (hydrostatic model). FIAs hosted in TOGM such as cassiterite (salinities of 2 wt% - 10 wt% and Th of 220˚C - 340˚C) helped set up the possible temperature limit of SGM (Cu sulfide) precipitations that are

estimated below 200˚C.

Keywords

Mokama Granites, Petrography, Geochemistry, Cu-Mineralization, XRF, EPMA, LA-ICP-MS, Fluid Inclusion Microthermometry

1. Introduction

The KIB leucogranites originated from the partial melting "anatexis" of the crustal subducting slab during the Mesoproterozoic collision event between the Congo craton and the Tanzanian block [1]. These leucogranites are sources of numeral metals such as Sn, W, Nb, Ta, Li, REE, Fe, Zn, and Cu (**Figure 1**). The occurrences of tin oxide group minerals (TOGM), columbite group minerals (CGM) and sulfide group minerals (SGM, Cu mineralization) are typically associated with the post-collision differentiated leucogranites [2] [3]. The enrichment and increase in mobility of metals are ensured by incipient post-magmatic fluid processes such as fluid exsolution, fluid-rock interactions [2] [4], metasomatic reactions and fluid-fluid mixings (magmatic-meteoric) [5].

The KIB G4 granites are known for Sn-W mineralization (in the Maniema, Kivu, and great Katanga provinces) and even G4 (G5) pegmatitic granites host Nb-Ta (coltan) mineralization. Few pegmatites such as in the Manono host a huge amount of Li mineralization.

The Mesoproterozoic KIB is overridden by the Neoproterozoic Lufilian (Zambian belt) known for the occurrences of Cu-Cu mineralization [7] [8] [9].

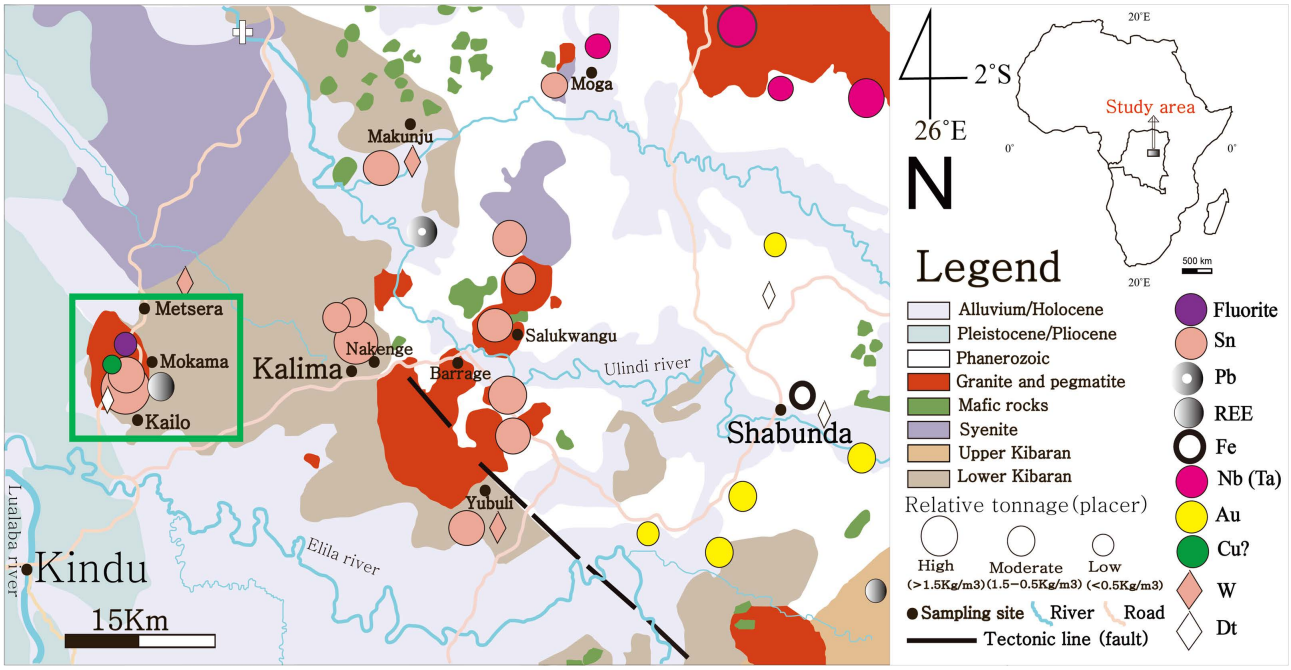

Figure 1. A geological map unit of the northern part of the KIB displaying the study area and sampling site (yellow rectangle) [6].

The sedimentary materials that filled up the aborted rift to form later on the Lufilian belt might come from pre-existing and eroded belt formation such as the Mesoproterozoic (Kibara belt, Karagwe-Ankole belt), Paleoproterozoic (Ubendian belt), Archean (Congo-Kasai craton, Bomu complex) [7].

The present study was conducted in the northern part of the KIB in Maniema province (DRC), and concerns the Mokama mineralized G4 granite that has intruded metasedimentary rocks (**Figure 1**) and hosting Cu mineralization. This study also tries to set in an unlikely possibility of the KIB Cu mineralization hosted in the granites or any other unknown (undiscovered) mafic or ultramafic rocks enriched in Cu-Co primary ores, to be the source (feeder) of the Lufilian sedimentary and stratiform Cu (Co) mineralization. This hypothesis incentivizes further studies to be done in order to demonstrate the link between the two above belts when it comes to Cu mineralization.

2. Geological Settings

The Mokama granite is located in the Maniema province in the Democratic Republic of Congo and makes part of the Kibara belt (KIB) and intrudes Mesoproterozoic metasediments made of essentially schists. The chemical-minera- logical-structural (CMS) classification of KIB granites showed three (3) main phases. The first phase is pre- to syn-tectonic and hosts less fractionated and "barren" granites (G1 - G3, Barrage site, **Figure 1**) and yield ages of 1100 - 1500 Ma. The second phase (this study) and the third phase are post-orogenic and host fractionated and "mineralized" granites (G4, Mokama site, **Figure 1**, **Figure 2**) and pegmatitic-granites (G4 - G5) of 950 - 1094 Ma [10] [11] [12]. Granites G1 - G3 are associated with the deformation D1 while granites G4 - G5 are associated with the deformation D2 (**Figure 2**) [6] [12].

3. Methodology

About 10 thin sections, 5 polished sections, and more than 50 doubly-sides polished sections (chips) have been prepared and observed under the polarizing microscope (Nikon, Japan) at Inha University (Incheon, Republic of Korea).

The electron probe microscope analysis (EPMA) was performed at Busan National University (Busan, Republic of Korea). This EPMA consisted of a JEOL-JXA-8530F PLUS model and used an acceleration voltage of 15 kV, an acceleration current of 40 nA, and an electron beam of 3 mm. The analysis was conducted with a peak duration of 10 s and a background time of 5 s. EPMA results are not provided here but are used for ore mineral identifications.

X-ray fluorescence (XRF, Zetium, Malvern Panalytical, United Kingdom) for major elements and Fusion ICP-MS for trace elements of the Mokama granite were performed at Activation Laboratories (Actlabs, Ontario, Canada). We have analyzed isotopes including ^{7}Li, ^{9}Be, ^{23}Na, ^{25}Mg, ^{27}Al, ^{29}Si, ^{39}K, ^{42}Ca, ^{45}Sc, ^{49}Ti, ^{51}V, ^{53}Cr, ^{55}Mn, ^{57}Fe, ^{59}Co, ^{61}Ni, ^{65}Cu, ^{66}Zn, ^{71}Ga, ^{73}Ge, ^{75}As, ^{85}Rb, ^{88}Sr, ^{89}Y, ^{90}Zr, ^{93}Nb, ^{95}Mo, ^{107}Ag, ^{111}Cd, ^{113}In, ^{118}Sn, ^{121}Sb, ^{133}Cs, ^{137}Ba, ^{139}La, ^{140}Ce, ^{141}Pr, ^{146}Nd, ^{147}Sm,

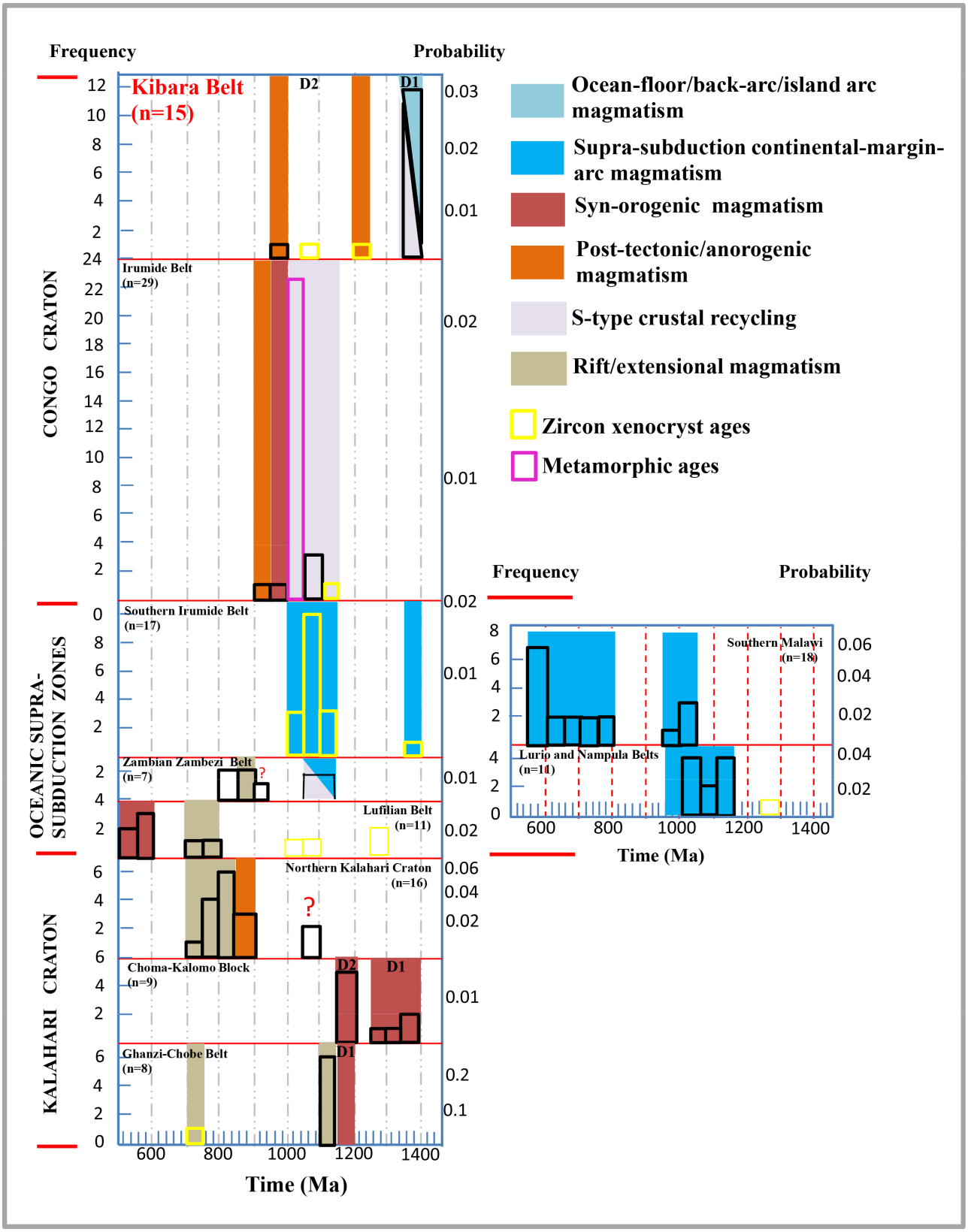

Figure 2. Sub-Saharan tectonic-chronostratigraphic and tectonic-magmatic units showing magmatic events associated with Mesoproterozoic syn-to post-orogenic belts. This study is part of the Kibara belt (KIB) granites associated with the deformation D2 [6].

^{151}Eu, ^{157}Gd, ^{159}Tb, ^{163}Dy, ^{165}Ho, ^{167}Er, ^{169}Tm, ^{173}Yb, ^{175}Lu, ^{178}Hf, ^{181}Ta, ^{182}W, ^{185}Re, ^{197}Au, ^{205}Tl, ^{208}Pb, ^{209}Bi, ^{232}Th, ^{238}U. A 193 nm Argon-Excimer laser (LA-NWR 193) was coupled with a quadrupole mass spectrometer Agilent 7700X. We have used a repetition rate of 5 Hz and a laser energy density of 3.5 - 6.0 J/cm^2. The laser beam diameter of the ablated zone was 50μm for the Mokam granitic slab. The fusion methods were utilized to ensure the total dissolution of the rock by acids. For the ICP-MS, the detection limits were Li (5ppm), Be (1 ppm), Na (100 ppm), Mg (100 ppm), Al (100 ppm), Si (100 ppm), K (100 ppm), Ca (100 ppm), Sc (1 ppm), Ti (10 ppm), V (5 ppm), Cr (20 ppm), Mn (10 ppm), Fe (100 ppm), Co (1 ppm), Ni (20 ppm), Cu (10 ppm), Zn (30 ppm), Ga (1 ppm), Ge (1 ppm), As (5 ppm), Rb (2 ppm), Sr (2 ppm), Y (1 ppm), 90Zr, Nb (1 ppm), Mo (2 ppm), Ag (0.5 ppm), Cd (excluded), In (0.2 ppm), Sn (1 ppm), Sb (0.5 ppm), Cs (0.5 ppm), Ba (2 ppm), La (0.1 ppm), Ce (0.1 ppm), Pr (0.05 ppm), Nd (0.1 ppm), Sm (0.1 ppm), Eu (0.05 ppm), Gd (0.1 ppm), Tb (0.1 ppm), Dy (0.1 ppm), Ho (0.1 ppm), Er (0.1 ppm), Tm (0.05 ppm), Yb (0.1 ppm), Lu (0.01 ppm), Hf (0.2 ppm), Ta (0.1 ppm), W (1 ppm), Re (1 ppm), Au (10 ppb), Tl (0.1 ppm), Pb (5 ppm), Bi (0.4 ppm), Th (0.1 ppm), U (0.1 ppm).

The fluid inclusion microthermometry was performed under the heating-cooling stage of Linkam-FTIR 600 which helped to determine ice melting temperature (Tm, ˚C) from which we have deduced the apparent salinity, and the total homogenization temperature (Th, ˚C) of fluid inclusions in the basis of H_2O-NaCl system. The stage calibration was performed using synthetic fluid inclusions (aqueous CO_2-CH_4 bearing inclusion and pure water inclusion) to obtain the triple point (−57.1˚C) of the CO_2-CH_4 mixed aqueous inclusion and ice melting (0.0˚C) and the critical homogenization temperature (374˚C) of the pure water inclusion. About 3 - 4 single inclusions per assemblage were measured and results were expressed as values of average ± standard deviation.

4. Results

4.1. Rock Petrography and Microscopic Observations

The Mokama Cu bearing granite (DMMOKA-2-7 and DMMOKA-2-9) descriptions of gangue and ore minerals were performed under petrographic and metallographic microscopes, and Raman spectroscopy at Inha and Seoul National Universities, and results showed the occurrences of Cu mineralization as sulfides and oxide ore minerals (**Figure 3**, **Figure 4**). The mineralogical compositions of the Mokama granites consist of mainly silicates. This Mokama granite showed a phaneritic texture and consists of quartz, biotite, muscovite, k-feldspar (orthoclase), plagioclases, pyroxene and amphibole (hornblende), and accessory minerals such as zircon, ilmenite, fluorite, topaz, magnetite, and ore minerals including tin oxide group (TOG: Sn-W), columbite group minerals (CGM: Nb-Ta), and sulfide group minerals (SGM: Cu-Zn-Fe-As). Some granites showed relatively big-sized grains (>1 cm) of euhedral quartz and flakes of micas (abundant muscovite, rare biotite), and these grain sizes could display a lateral variation

within the granitic body. Such rocks could be considered pegmatitic granites, they were rare and mineralized as well.

The Cu ore minerals (Table 1) consisted of essential chalcopyrite ($CuFeS_2$) that shows rims of chalcocite (Cu_2S), also lately replaced by covellite (CuS) and finally malachite ($Cu_2CO_3(OH)_2$) in the supergene zones (Figure 3(a), Figure 3(b), Figure 4(f)). The alteration that affected the KIB mineralized granites (especially in the mineralized Mokama granite, Figure 3(c)) consisted of quartz ± muscovite ± albite (± sericite) whereas the KIB barren granites showed quartz ± pyrite ± fluorite (± chlorite) (Figure 3(d)) or quartz ± albite ± chlorite. The presence and abundance of muscovite can be interpreted as an acidic environment where feldspars were transformed into muscovite (Figure 3(c)) [6].

The barren granites (from the Barrage site, Figure 1) show abundant euhedral quartz grains and pinkish K-feldspar (orthoclase), while biotite, Fe-oxides, pyroxenes, and amphiboles are accessory minerals.

The Cu mineralization of the Mokama G4 granite in the Mesoproterozoic KIB is considered a late-stage magmatic-hydrothermal sulfide and disseminated

Table 1. Ore mineral associations and paragenetic sequences in the Mokama granite and peri-granitic quartz veins.

Mineral	Pre-ore stage (I)	Oxide stage (II) (Sn, W, Nb, Ta)		Sulfide stage (III) (Cu-Zn-As-Fe)		Supergene (IV)
		Early	Late	Early	Late	
Cassiterite						
Wolframite						
Pyrite						
Arsenopyrite						
Chalcopyrite						
Columbo-tantalite						
Molybdenite						
Pyrrhotite						
Sphalerite						
Chalcocite						
Covellite						
Quartz						
Fluorite						
Malachite						
Magnetite						
Hematite						
Goethite						
Calcite						
Barite						

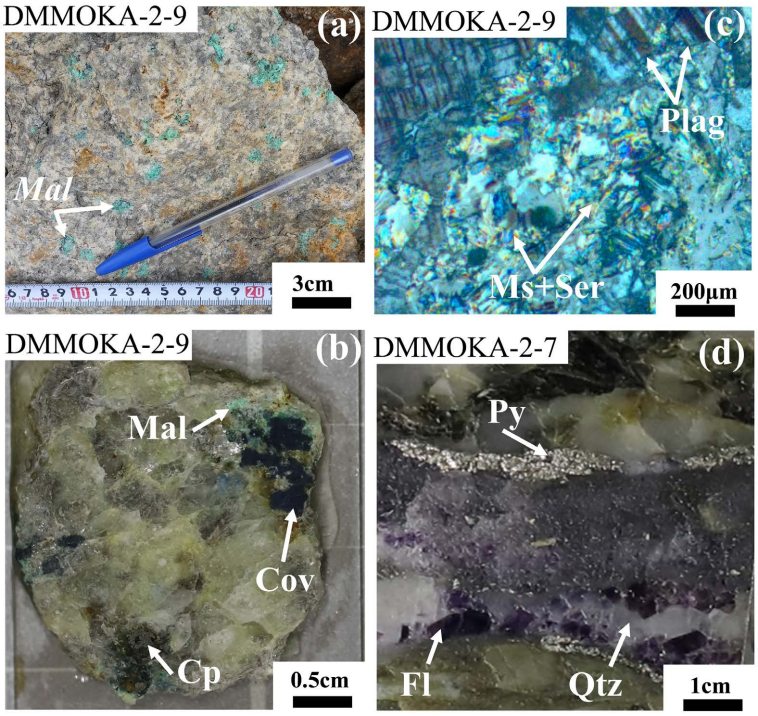

Figure 3. ((a), (b)) Photo macrographs of the Mokama (DMMOKA-2-9) mineralized granite showing Cu mineralization; (c) Photomicrograph (XPL) of the Mokama granite displaying the hydrothermal alteration of feldspar to muscovite; (d) Photo macrograph of the Mokama (DMMOKA-2-7) granite displaying quartz-pyrite-fluorite in a quartz vein.

within the granitic rock compared to the sedimentary stratiform (and vein-type) Cu-Co of the Neoproterozoic Lufilian belt (LUB) in the great Katanga province In DRC [9] [13] [14]. In the KIB Mokama granites, the hypogene ore mineralization consisted of bornite, sphalerite, pyrite and chalcopyrite (**Figures 4(a)-(e)**). Bornite and chalcopyrite showed rims that are due to the later replacement by supergene sulfides such as chalcocite and covellite (**Figures 4(a)-(c)**), and these last ones were later on replaced by oxides such as the green mass of malachite (**Figure 4(f)**). Some sphalerite grains showed chalcopyrite diseases (**Figure 4(d)** & **Figure 4(e)**) and inclusions of silicate minerals (**Figure 4(e)**) that can be interpreted as associated with relatively high temperature-derived fluids. The occurrence of arsenopyrite is more likely associated with hydrothermal environment.

4.2. Rock Geochemistry

The Mokama G4 granites chemistry (XRF, LA-ICP-MS, **Table 2**) showed SiO_2 (71 wt% - 79 wt%), ASI (1.38 - 3.12 molar), and enriched in Rb (681 - 1000 ppm), Ta (12 - 151 ppm), Sn (43 - 142 ppm), Cu (10 - 4300 ppm), Zn (60 - 740 ppm), U (2.2 - 20.7 ppm) while depleted in Zr (20 –31 ppm), Sr (20 - 69 ppm), Hf (1.3 - 2.0 ppm), Th (2.2 - 18.9 ppm), W (9 - 113 ppm), Pb (5 - 50 ppm), Ge (5 - 10 ppm), Cs (21 - 53 ppm), and Bi (0.6 - 17.4 ppm). The Aluminum saturation index (ASI = 1.7 - 3.1) showed that this Mokama G4 granite can be considered a

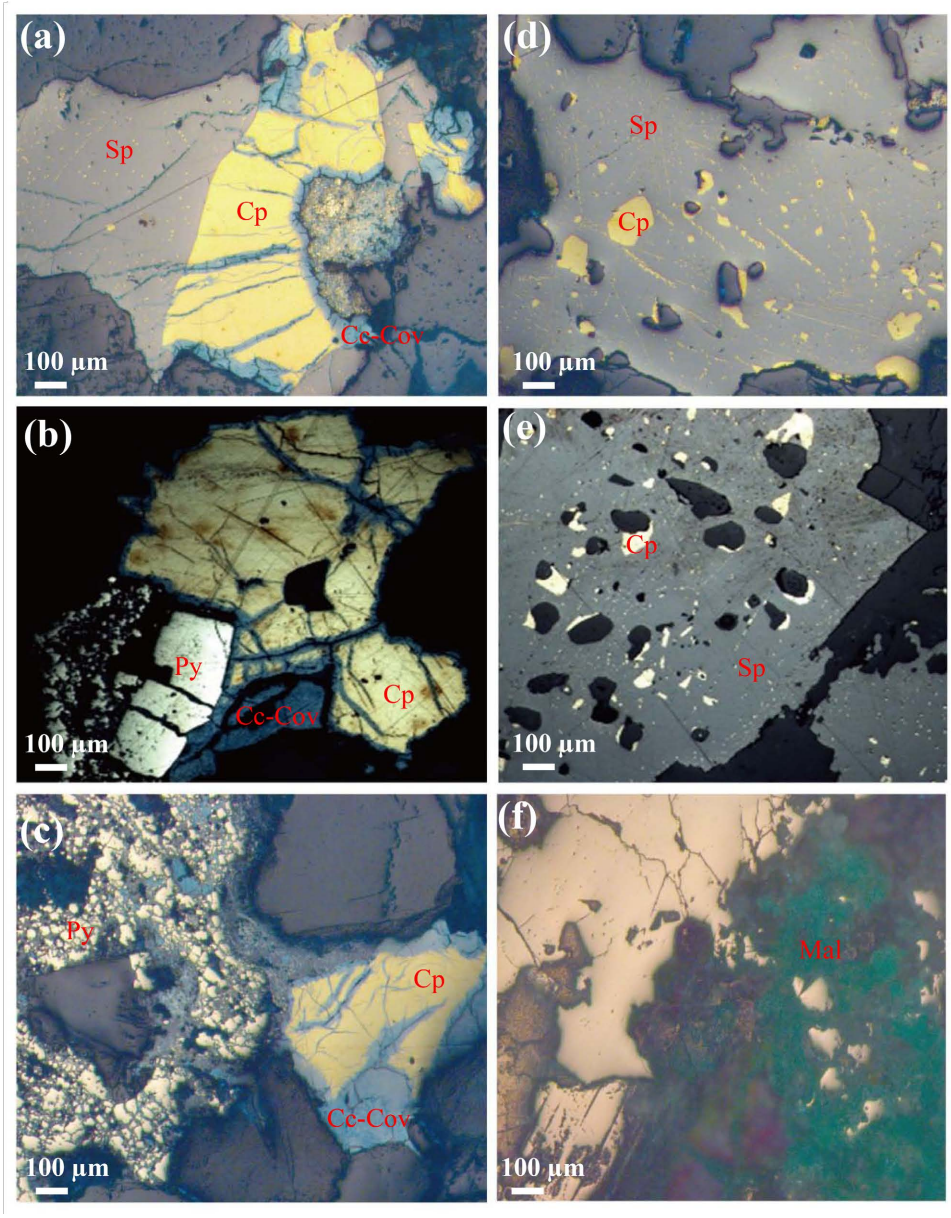

Figure 4. (a)-(d) Photomicrographs (PPL) of the Mokama (DMMOKA-2-9) mineralized granite displaying the presence of sphalerite (SP), chalcopyrite [15], pyrite (Py), chalcocite (Cc), and covellite (Cov); (e) A photomicrograph (PPL) of sphalerite (Sp) showing inclusions of chalcopyrite and silicates from the Mokama site (DRC; (f) A photomicrograph (PPL) of the Mokama G4 granite showing green mass of malachite (Mal). The sphalerite displays in (a), (d), and (e) chalcopyrite disease features.

peraluminous S-type leucogranites (**Figures 5(a)-(c)**), ferroan, highly potassic and calc-alkalitic. This Mokama granite is a late (post)-collisional granitoid, and is characterized by high Rb/Sr, Cu/As, Zn/As and $(Ta/Zr)_N$; and low (La/Yb) and Ba/Sr. This rock is also relatively enriched in Rb, Ta, Sn, Cu and REE (mostly HREE which are fractionated by pyroxenes and amphiboles). The ratios $(La/Sm)_N$, $(La/Yb)_N$, $(Gd/Yb)_N$, $(Ta/Zr)_N$ and $(Eu/Eu^*)_N$ are 2.9 - 10.1, 0.1 - 11.5, 0.1 - 0.8, 113.3 - 2120.7, and 0.1 - 1.5 respectively.

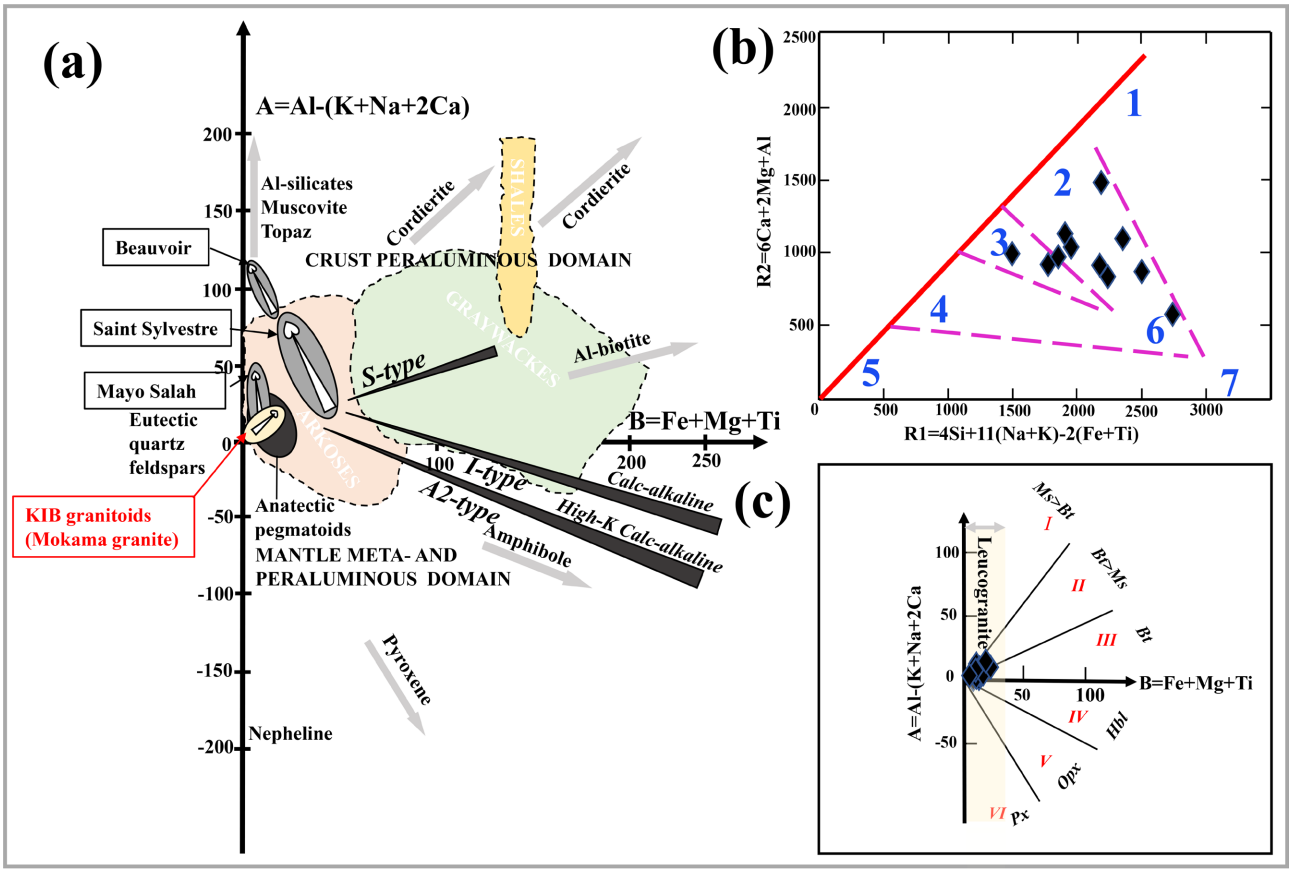

Figure 5. Multicationic plots of KIB granitoid (Mokama) the Maniema province (D.R.C); ((a), (c)) B (=Fe + Mg + Ti) vs A (=Al-(K + Na + 2Ca) (b) R1 = (4Si + 11 (Na + K) − 2 (Fe + Ti)) vs R2 = (6Ca + 2Mg + Al) (I = Muscovite > Biotite, II = Biotite > Muscovite, III = Biotite, IV = Hornblende, V = Orthopyroxene, VI = Clinopyroxene), (**1**-Mantle fractionates, **2**-Pre-plate collision, **3**-Post-collision Uplift, **4**-Late orogenic, **5**-Anorogenic, **6**-Syn-collision, **7**-post-ororgenic).

4.3. Ore Mineral Associations and Paragenetic Sequences

The Kibara belt mineralized granites (granite s.s., pegmatite, peri-granitic quartz veins) in general and the Mokama granite in particular started by the precipitation of TOG, followed by CGM and ended with SGM of non-economic deposits.

4.4. Fluid Inclusions and Microthermometric Measurements

(ID-inclusions), and CO_2-rich fluid inclusions (**Figure 6(a)** & **Figure 6(b)**). The microthermometric measurements (Linkam-FTIR 600, Inha University) were carried out essentially on fluid inclusions assemblages (FIAs) hosted in quartz, and consisted of liquid-rich and ID as of primary and pseudo-secondary fluid inclusions (**Figure 6(a)** & **Figure 6(b)**).

The results of fluid microthermometry can be used to determine the paleo-depths and thermodynamic conditions (apparent salinity, homogenization temperature and pressure) of rocks and ore minerals as well [6] [16]. Microthermometric results (**Table 3**) of fluid inclusion assemblages (FIAs) hosted in quartz in the Mokama granite show ranges of salinities of 4 wt% - 23 wt% (NaCl equivalent)

Table 2. Major and trace element compositions of the Kibara belt (KIB) mineralized granitic intrusions and the host rock (schist). Major elements (expressed in wt%) were analyzed by XRF while trace elements (expressed in ppm) by Fusion ICP-MS methods.

Oxides (wt%)	Method Code	Monzo granite	Monzo granite	Quartz rich granitoid	Alkali feldspar granite	Quartz rich granitoid	Quartz rich granitoid	Schist (Host rock)
		DMMOKA -2-1	DMMOKA -2-5	DMMOKA -2-6	DMMOKA -2-7	DMMOKA -2-8	DMMOKA -2-9	DMYUB -2
SiO_2	XRF	71.56	71.66	73.99	71.84	76.35	76.6	49.96
TiO_2	XRF	0.08	0.01	0.03	0.02	0.03	0.03	0.83
Al_2O_3	XRF	17.46	16.09	13.74	17.75	12.78	13.87	26.65
Fe_2O_3t	XRF	2.97	1.51	4.2	1.95	2.34	2.81	5.96
MnO	XRF	0.18	0.07	0.23	0.19	0.11	0.12	0.15
MgO	XRF	0.07	0.03	0.02	0.03	0.08	0.06	2.78
CaO	XRF	0.61	0.23	0.71	0.49	1.97	0.05	0.06
Na_2O	XRF	2.82	4.05	0.4	0.09	0.1	0.11	0.39
K_2O	XRF	3.22	4.22	3.82	5.51	3.55	3.86	7.66
P_2O_5	XRF	0.37	0.15	0.18	0.19	0.5	0.01	0.06
LOI	XRF	1.44	1.03	1.75	2.4	1.85	1.76	3.87
TOTAL		100.8	99.1	99.1	100.5	99.7	99.3	98.4
Traces (ppm)								
V	FUS-ICP	5	5	5	5	5	5	112
Cr	FUS-MS	20	20	20	20	20	20	100
Co	FUS-MS	1	1	1	1	1	1	3
Ni	FUS-MS	20	20	20	20	20	20	30
Ba	FUS-ICP	26	159	55	49	38	79	1122
Rb	FUS-MS	962	681	1000	1000	696	876	1000
Sr	FUS-ICP	23	30	69	25	51	20	117
Zr	FUS-ICP	31	22	21	20	20	20	180
Y	FUS-ICP	10	49	1	4	3	1	24
Nb	FUS-MS	37	40	36	43	88	34	13
Ta	FUS-MS	12.5	19.4	39.9	17.3	151	48	1.5
Hf	FUS-MS	1.3	1.3	1.8	1.2	2	1.7	4.5
Th	FUS-MS	4.2	2.2	10.3	3.5	6.4	7.3	18.9
U	FUS-MS	20.7	9.7	5.9	2.2	5.9	4.9	2.4
La	FUS-MS	6.6	1.4	1.6	1.4	2.2	1.7	66.3
Ce	FUS-MS	15.4	2.7	2.8	2.7	2.8	2.6	138
Pr	FUS-MS	1.8	0.29	0.26	0.28	0.26	0.26	14.3
Nd	FUS-MS	6.1	1	0.8	0.9	0.7	0.9	49.6

Continued

Sm	FUS-MS	1.4	0.3	0.1	0.2	0.2	0.2	8.3
Eu	FUS-MS	0.05	0.08	0.05	0.08	0.06	0.05	1.57
Gd	FUS-MS	0.9	1.1	0.1	0.3	0.2	0.1	5.5
Tb	FUS-MS	0.2	0.4	0.1	0.1	0.1	0.1	0.8
Dy	FUS-MS	1.5	4.2	0.1	0.4	0.3	0.1	4.6
Ho	FUS-MS	0.3	1.1	0.1	0.1	0.1	0.1	0.8
Er	FUS-MS	1	4.3	0.1	0.3	0.2	0.1	2.5
Tm	FUS-MS	0.18	0.88	0.05	0.07	0.05	0.05	0.4
Yb	FUS-MS	1.3	6.7	0.1	0.6	0.4	0.1	2.5
Lu	FUS-MS	0.2	1.08	0.01	0.1	0.09	0.01	0.37
As	FUS-MS	5	5	5	5	5	5	48
Be	FUS-ICP	7	5	7	4	5	6	16
Mo	FUS-MS	8	2	3	2	2	2	2
Sn	FUS-MS	121	43	142	53	88	87	134
W	FUS-MS	14	19	113	9	36	36	60
Bi	FUS-MS	7.7	3.7	17.4	0.6	16.9	10.7	0.4
Cd	—	—	—	—	—	—	—	—
Cs	FUS-MS	42.3	21.4	53.4	33.7	29.5	38.5	752
In	FUS-MS	0.2	0.2	0.4	0.2	0.2	0.6	0.2
Sb	FUS-MS	0.5	0.5	0.5	0.5	0.5	0.5	0.5
Cu	FUS-MS	10	20	330	30	330	4300	10
Pb	FUS-MS	31	27	50	5	9	8	539
Ga	FUS-MS	32	28	27	29	23	26	26
Ge	FUS-MS	10	5	9	2	6	8	5
Li	—	—	—	—	—	—	—	—
Zn	FUS-MS	240	130	740	60	160	570	100
Tl	FUS-MS	4.4	4	4.8	6.8	3.5	4.3	5.8
Sc	FUS-ICP	1	1	1	1	1	1	20
Ag	FUS-MS	0.5	1	1.2	0.5	0.5	0.5	0.7
$(La/Sm)_N$		3.0	2.9	10.1	4.4	6.9	5.4	-
$(La/Yb)_N$		3.4	0.14	10.8	1.6	3.7	11.5	-
$(Gd/Yb)_N$		0.6	0.1	0.8	0.4	0.4	0.8	-
$(Ta/Zr)_N$		113.3	247.7	533.7	243.0	2120.7	674.1	-
$(Eu/Eu^*)_N$		0.135	0.426	1.500	1.000	0.920	1.056	-

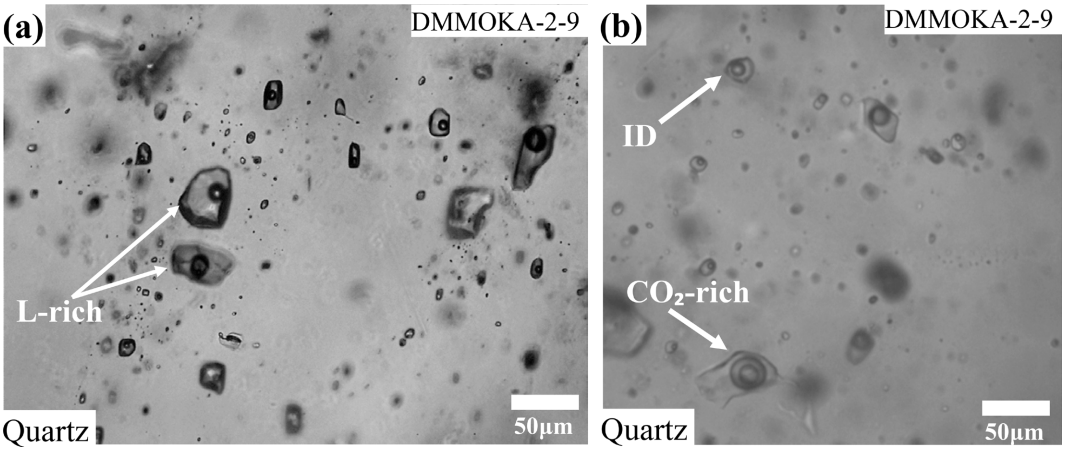

Figure 6. (a) Photomicrographs (PPL) of liquid-rich and ID fluid inclusions hosted in quartz in mineralized granite from the Mokama (DMMOKA-2-9) site in DRC; (b) Photomicrographs (PPL) of CO_2-rich and ID fluid inclusions hosted in quartz in mineralized granite from the Mokama (DMMOKA-2-9) site in DRC.

Table 3. Fluid inclusion microthermometric results of the Mokama granites in the KIB (FIAs = fluid inclusion assemblages, wherein 3 to 4 single inclusions per assemblage)Quartz_Barren granite (n = 25 FIAs).

	Salinity (wt% NaCl equiv.)	T_h (˚C)	P (bar)	Depth (km)	Density (g/cm³)
Max.	22.7	368.9	181.7	0.69	1.040
Min.	2.7	123.0	2.0	0.01	0.786
Avg.	14.3	275.7	88.3	0.33	0.888
Std.	6.3	91.9	64.2	0.24	0.068
Quartz_Mineralized G4 granite (n = 55 FIAs)					
Max.	23.1	548.4	736.9	2.79	1.027
Min.	3.8	185.3	10.1	0.04	0.627
Avg.	14.3	308.7	135.0	0.51	0.851
Std.	5.9	87.7	173.9	0.66	0.097
Quartz_Mineralized G4 pegmatite (n = 9 FIAs)					
Max.	12.2	326.5	115.6	0.44	0.982
Min.	6.6	179.3	9.0	0.03	0.788
Avg.	9.3	241.1	43.4	0.16	0.887
Std.	1.7	51.3	38.4	0.15	0.066
Quartz_Mineralized greisen (n = 6 FIAs)					
Max.	18.8	500.8	578.1	2.18	0.889
Min.	11.3	259.6	43.5	0.16	0.654
Avg.	11.3	348.0	200.3	0.76	0.889
Std.	3.5	89.8	193.8	0.73	0.087

and homogenization temperatures (Th) of 190˚C - 550˚C. A boiling assemblage in the granite suggests a fluid phase separation occurred at about 380 - 610 bars, and this corresponds to apparent paleodepths of approximately 1 - 2 km (lithostatic model) or 3 - 5 km (hydrostatic model). FIAs hosted in cassiterite (salinities of 2 wt% - 10 wt% and Th of 220˚C - 340˚C) set up the upper limit of SGM including Cu (-Fe-Zn-As) sulfides that probably precipitated at temperatures below 200˚C (**Figure 7(a)** & **Figure 7(b)**).

5. Discussions

5.1. The Mokama Mineralized Granite Genesis, Metal Mobilities, and Mineralization Processes

The Mokama G4 granites are peraluminous rocks associated with the Kibaran collisional event, and host huge critical and base metal potentials [10] [12] [18]. The magmatic-hydrothermal fluid processes that affected these granitic intrusions enable the mobility of elements and their precipitations inside and outside (country rock as hydrothermal veins) of the granitic intrusions. This is in consideration of many facts including the circulation of rising hot magmatic-hydrothermal reduced geofluids enriched in metal complexes (mostly chlorine and fluorine ligands, and rarely hydroxyl ligands), fluid-rock interactions with remobilization of metals from the host/country rock (lithologic control), mixing of fluids (hot saline magmatic-hydrothermal and cooler less saline meteoric waters) that possibly induced the oxidization, cooling-fugacity controls, and alteration that might be influenced and controlled the pH [6].

Fluid inclusion data (quartz, cassiterite, fluorite) and the ore chemistry (oscillatory cassiterite, wolframite) showed that the TOGM (such as Sn-W) precipitated earlier, then followed by CGM (such as Nb, Ta, Li), and finally SGM (such

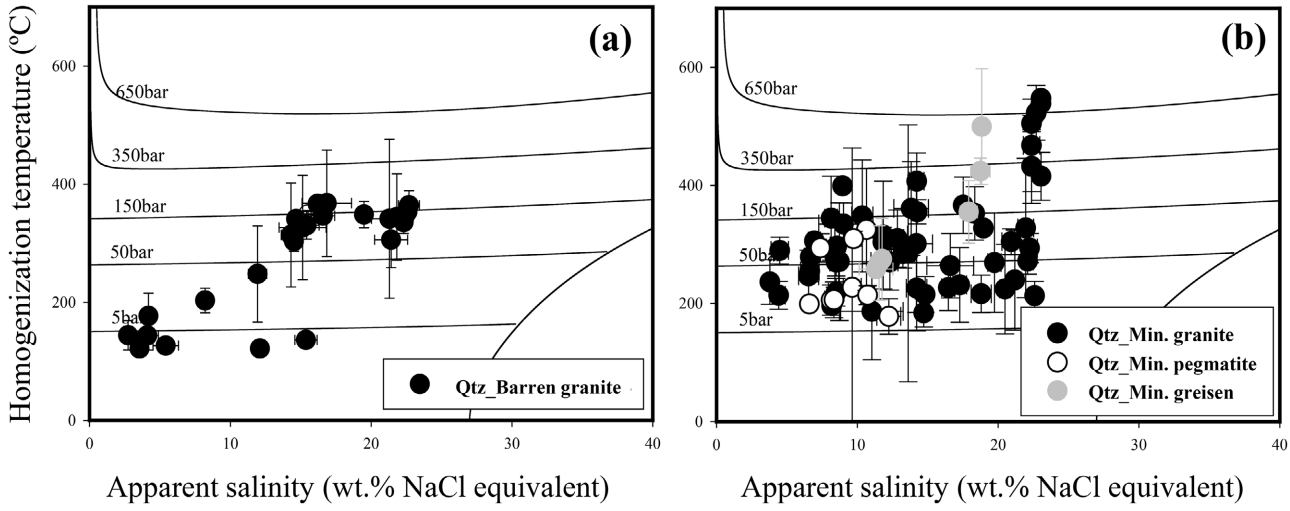

Figure 7. Plots of homogenization temperatures (T_h) versus apparent salinities of fluid inclusions hosted quartz from respectively Barren granites (Barrage site, **Figure 1**) and Mineralized granites (Mokama site, **Figure 1**) in DRC. The isobaric curves and salinities were constrained by using a H_2O-NaCl model [17]. Results are reported as averages and standard deviations (Avg ± σ1) calculated from 3 - 4 single measured inclusions.

as Cu, Zn, As, Fe) that occurred at the very last stage. In the KIB, TOGM and CGM deposits are economically valuable whereas SGM is still now of non-economic value.

5.2. The KIB Magmatic-Hydrothermal Cu Bearing Granites as an Unlikely Potential Source of the Sedimentary Lufilian Cu Mineralization

The KIB hosts Cu mineralization associated with magmatic-hydrothermal processes, and the LUB has Cu (Co) mineralization related to sedimentary (multi-source materials) processes. The Katanga supergroup relies directly on the KIB basement and has no compelled data and evidence that show the possible material connection between the two belts. Some researchers showed that the LUB sediments originated from many sources from Precambrian and Archean formations [7] [8] [9] [13]. A few questions remained unsolved especially when it comes to addressing the source of Cu and Cu mineralization. The occurrence of Cu mineralization in the KIB belt could possibly be the primary Cu feeder of the LUB by the remobilization of rising mineralizing fluids through the Katanga basin. The fact that the LUB is characterizable by Cu-Co deposits, makes the possibility of considering the KIB as Cu feeder very inconsistent and diminished. The best feeder of both Cu-Co metals would be intrusive mafic or ultramafic rocks; and in the nearby LUB area, such rocks have not been discovered or well documented. Another very unlikely source of LUB Co could be ultramafic dyke (peridotites) intrusions in the Archean Congo-Kasai craton that formed lately serpentinized bodies hosting Ni-Cr (with by Co-V-Zn as by products) in the regolith zones (such as in the Lutshatsha, Mfwamba, and Nkonko massifs) [19]. None of the above hypotheses or scenarios has been proven until today. Thus, despite some attempts to grasp the origin of Cu, the primary source of Co in the LUB remains totally unknown and requires more studies in the future.

6. Conclusion

The Mokama G4 leucogranite in the KIB hosts disseminated mineralization of Cu, and the essential ore minerals are composed of chalcopyrite, chalcocite, covellite and malachite. The hydrothermal pervasive alteration of quartz-muscovite-albite in the Kibara belt contributed to metal mobilities during fluid-rock interactions. Fluid inclusion results showed that this granite was emplaced at 2 - 5 km deeper as paleodepths, the TOGM (and CGM) precipitated earlier at relatively high temperatures (>200˚C) whereas SGM precipitated later at probably below 200˚C. This Mesoproterozoic KIB Cu mineralization could unlikely is the source (feeder) of the Neoproterozoic Lufilian Cu (Co) stratiform mineralization. We recommend more studies to be done in order to establish a possible existence or not of link between the two belts Cu mineralization.

Author Contributions

The Conception of the project, D.K.M.; field works and sampling, D.K.M., J.P.B.,

P.K.K., and F.M.M.; petrographic and geochemical analyses (EPMA, LA-ICPMS, Raman spectroscopy, and fluid inclusion microthermometry), D.K.M., I.B, C.M.M., and F.M.M.; data validation and curation, D.K.M. and J.P.B.; writing—original draft preparation, D.K.M.; writing—review, editing, D.K.M. and F.M.M.; supervision, D.K.M.; funding acquisition, D.K.M. All authors have read and agreed to the published version of the manuscript.

Fundings

The present study received financial support from the National Institute for International Education and Development (NIIED-2020, grant number NIIED-200807-0012) in the Republic of Korea (D.K.M.) and the BEBUC-Kroëner Foundations for sample transportation.

Acknowledgements

We sincerely thank Jung Hun Seo, Insung Lee, Sangki Kwon, Kanika Mayena Thomas, Makutu Ma Ngwayaya, and Ongendangenda Tienge Albert for constructive discussions related to this study. Thanks to Junhee Lee, TongHa Lee, Yevgeniya Kim, Yuri Choi, Hahyeon Park, Yechan Jeon, and Dedel Milikwini for the material and sample preparations.

Conflicts of Interest

The authors declare no conflicts of interest regarding the publication of this paper.

References

[1] Chen, Y., Song, S., Niu, Y. and Wei, C. (2014) Melting of Continental Crust during Subduction Initiation: A Case Study from the Chaidanuo Peraluminous Granite in the North Qilian Suture Zone. *Geochimica and Cosmochimica Acta*, **132**, 311-336. https://doi.org/10.1016/j.gca.2014.02.011

[2] Hulsbosch, N., Boiron, M.C., Dewaele, S. and Muchez, P. (2016) Fluid Fractionation of Tungsten during Granite-Pegmatite Differentiation and the Metal Source of Peribatholitic W Quartz Veins: Evidence from the Karagwe-Ankole Belt (Rwanda). *Geochimica and Cosmochimica Acta*, **175**, 299-318. https://doi.org/10.1016/j.gca.2015.11.020

[3] Hulsbosch, N. and Muchez, P. (2020) Tracing Fluid Saturation during Pegmatite Differentiation by Studying the Fluid Inclusion Evolution and Multiphase Cassiterite Mineralisation of the Gatumba Pegmatite Dyke System (NW Rwanda). *Lithos*, **354-355**, 1-26. https://doi.org/10.1016/j.lithos.2019.105285

[4] Che, X.D., Linnen, R.L., Wang, R.C., Aseri, A. and Thibault, Y. (2013) Tungsten Solubility in Evolved Granitic Melts: An Evaluation of Magmatic Wolframite. *Geochimica and Cosmochimica Acta*, **106**, 84-98. https://doi.org/10.1016/j.gca.2012.12.007

[5] Audétat, A. (2019) The Metal Content of Magmatic-Hydrothermal Fluids and Its Relationship to Mineralization Potential. *Economic Geology*, **114**, 1033-1056. https://doi.org/10.5382/econgeo.4673

[6] Makutu, D.K., Seo, J.H., Lee, I., Oh, J., Kang, P., Ongendangenda, A.T. and Makoka,

F.M. (2023) Magmatic-Hydrothermal Fluid Processes of the Sn-W Granites in the Maniema Province of the Kibara Belt (KIB), Democratic Republic of Congo. *Minerals*, **13**, 1-36. https://doi.org/10.3390/min13040458.

[7] Mambwe, P., Delpomdor, F., Lavoie, S., Mukonki, P., Batumike, J. and Muchez, P. (2020) Sedimentary Evolution and Stratigraphy of the Similar to 765-740 Ma Kansuki-Mwashya Platform Succession in the Tenke-Fungurume Mining District, Democratic Republic of the Congo. *Geologica Belgica*, **23**, 69-85. https://doi.org/10.20341/gb.2020.022

[8] Mambwe, P., Kipata, L., Chabu, M., Muchez, P., Lubala, T., Jebrak, M. and Delvaux, D. (2017) Sedimentology of the Shangoluwe Breccias and Timing of the Cu Mineralisation (Katanga Supergroup, D. R. of Congo). *Journal of African Earth Sciences*, **132**, 1-15. https://doi.org/10.1016/j.jafrearsci.2017.04.017

[9] Mambwe, P., Milan, L., Batumike, J., Lavoie, S., Jebrak, M., Kipata, L., Chabu, M., Mulongo, S., Lubala, T., Delvaux, D. and Muchez, P. (2017) Lithology, Petrography and Cu Occurrence of the Neoproterozoic Glacial Mwale Formation at the Shanika Syncline (Tenke Fungurume, Congo Copperbelt; Democratic Republic of Congo). *Journal of African Earth Sciences*, **129**, 898-909. https://doi.org/10.1016/j.jafrearsci.2017.02.021

[10] Dewaele, S., Hulsbosch, N., Cryns, Y., Boyce, A., Burgess, R.A. and Muchez, P. (2016) Geological Setting and Timing of the World-Class Sn, Nb-Ta and Li Mineralization of Manono-Kitotolo (Katanga, Democratic Republic of Congo). *Ore Geology Reviews*, **72**, 373-390. https://doi.org/10.1016/j.oregeorev.2015.07.004

[11] Hulsbosch, N. (2019) Nb-Ta-Sn-W Distribution in Granite-related Ore Systems. In: Decrée, S. and Robb, L., Eds., *Ore Deposits*: *Origin*, *Exploration*, *and Exploitation*- John Wiley and Sons, Hoboken, 75-107. https://doi.org/10.1002/9781119290544.ch4

[12] Pohl, W., Biryabarema, M.A. and Lehmann, B. (2013) Early Neoproterozoic Rare Metal (Sn, Ta, W) and Gold Metallogeny of the Central Africa Region: A Review. *Applied Earth Science*, **122**, 66-82. https://doi.org/10.1179/1743275813Y.0000000033

[13] Dewaele, S., Muchez, P., Vets, J., Fernandez-Alonzo, M. and Tack, L. (2006) Multiphase Origin of the Cu-Co Ore Deposits in the Western Part of the Lufilian Fold-and-Thrust Belt, Katanga (Democratic Republic of Congo). *Journal of African Earth Sciences*, **46**, 455-469. https://doi.org/10.1016/j.jafrearsci.2006.08.002

[14] Haest, M., Muchez, P., Dewaele, S., Boyce, A.J., von Quadt, A. and Schneider, J. (2009) Petrographic, Fluid Inclusion and Isotopic Study of the Dikulushi Cu-Ag Deposit, Katanga (DRC): Implications for Exploration. *Mineralium Deposita*, **44**, 505-522. https://doi.org/10.1007/s00126-009-0230-x

[15] Agangi, A., Kamenetsky, V.S. and McPhie, J. (**2010**) The Role of Fluorine in the Concentration and Transport of Lithophile Trace Elements in felsic Magmas: Insights from the Gawler Range Volcanics, South Australia. *Chemical Geology*, **273**, 314-325. https://doi.org/10.1016/j.chemgeo.2010.03.008

[16] Seo, J.H., Kim, Y., Lee, T. and Guillong, M. (2021) Periodically Released Magmatic Fluids Create a Texture of Unidirectional Solidification (UST) in Ore-Forming Granite: A Fluid and Melt Inclusion Study of W-Mo Forming Sannae-Eonyang Granite, Korea. *Minerals*, **11**, 1-22. https://doi.org/10.3390/min11080888

[17] Bodnar, R.J.A. and Vityk, M.O. (1994) Interpretation of Microthermometric Data for H2O-NaCl Fluid Inclusions. *Virginia Tech*, 117-130.

[18] Dewaele, S., DeClerq, F., Muchez, P., Schneider, J., Burgess, R., Boyce, A. and Fer-

nandez-Alonso, M. (2010) Geology of the Cassiterite Mineralisation in the Rutongo Area, Rwanda (Central Africa): Current State of Knowledge. *Geologica Belgica*, **13,** 91-112.

[19] Herman, P. and Raucq, P. (1962) Données complémentaires sur les chromites du Kasaï. *Bulletin de la Société Belge de Géologie, de Paléontologie et d'Hydrologie*, 336-357.